Supporting Information for Seismic and aseismic fault slip during the initiation phase of the 2017 $M_W = 6.9$ Valparaíso earthquake

Emmanuel Caballero[1], Agnès Chounet[1], Zacharie Duputel[1], Jorge Jara[2],

Cedric Twardzik[1], Romain Jolivet[2,3]

[1]Institut de Physique du Globe de Strasbourg, UMR 7516, Université de Strasbourg/EOST, CNRS, Strasbourg, France.

[2]Laboratoire de Géologie, Département de Géosciences, École Normale Supérieure, PSL Université, CNRS UMR 8538, Paris, France

[3]Institut Universitaire de France, 1 rue Descartes, 75005 Paris, France

Contents of this file

Introduction

S1. GPS proccesing

68 continuous GPS (cGPS) were processed in South America (66 stations) and Nazca (2 stations) Plates (Figures S1 and S2), from different networks that are listed below:

• 13 cGPS from the International GNSS service (`www.igs.org`): ANTC, AREQ, BRAZ, BRFT, CHPI, GLPS, ISPA, KOUR, LPGS, RIO2, SANT, UFPR, UNSA.

• 3 cGPS from the Instituto Geográfico Militar of Bolivia (`www.igmbolivia.gob.bo`): SCRZ, URUS, YCBA.

• 11 cGPS from the Brazilian Network (RBMC-IP, `www.ibge.gov.br`): CUIB, MABA, MSCG, NAUS, POAL, POVE, PRCV, ROCD, RSAL, SAVO, TOPL.

• 15 cGPS from Argentian National Network (RAMSAC, `www.ign.gob.ar` (Piñón et al., 2018)) AZUL, BCAR, CATA, DINO, EBYP, ESQU, MA01, NESA, PEJO, RWSN, SL01, TUCU, UNRO, UNSJ, VBCA

• 5 cGPS from the Chilean - French cooperation through LIA "Montessus de Ballore" (`www.lia-mb.net`): CONS, JRGN, OVLL, UAPE, UDAT.

• 2 cGPS from the Ministerio de Bienes Nacionales of Chile (`www.bienesnacionales.cl`): BN05, BN13

• 18 cGPS from the Centro Sismológico Nacional de Chile (CSN, `www.csn.uchile.cl` (Báez et al., 2018)): CHDA, CTPC, CUVI, DGF1, LVIL, MPLA, NAVI, PORT, QTAY, RCSD, ROB1, QTAY, SLMC, TLGT, TRPD, UAIB, VALN, ZAPA.

All these data were processed in double differences using GAMIT 10.7 software to obtain daily, 12 and 6 hours estimates of station positions, choosing ionosphere-free combination and fixing the ambiguities to integer values. The precise orbits from the International

GNSS Service for Geodynamics, precise EOPs from the IERS bulletin B, IGS tables to describe the phase centers of the antennas, FES2004 ocean-tidal loading corrections, as well as atmospheric loading corrections (tidal and non-tidal). We used precise orbits from the International GNSS Service for Geodynamics, precise EOPs from the IERS bulletin B, IGS tables to describe the phase centers of the antennas, FES2004 ocean-tidal loading corrections, as well as atmospheric loading corrections (tidal and non-tidal). One tropospheric vertical delay parameter and two horizontal gradients per stations are estimated every 2 hours. Daily solutions and position time series are combined using the PYACS software (Nocquet, 2017) in a regional stabilization process. The results are mapped into ITRF 2014 reference frame (Altamimi et al., 2016) and then put in the South-American frame using the Euler pole at -83.4° E, 15.2° N, and angular velocity $0.287^\circ \mathrm{my}^{-1}$ (Nocquet et al., 2014).

S2. Prediction error covariance matrix

We focus on prediction uncertainties due to inaccuracies in the Earth model. These uncertainties are represented by the matrix $\mathbf{C_p}$. We note the forward model $\mathbf{g}(\mathbf{\Psi}, \mathbf{m})$ for a source model $\mathbf{m}$, and Earth model parameters $\mathbf{\Psi}$ (i.e., P and S wave velocities, density). We can estimate $\mathbf{C_p}$ empirically from an ensemble of random models $\mathbf{\Psi_i}, (i = 1, \ldots, n)$ as:

$$\mathbf{C_p} = \frac{1}{n-1} \sum_{i=1}^{n} (\mathbf{g}(\mathbf{\Psi_i}, \mathbf{m}) - \bar{\mathbf{g}}(\mathbf{\Psi}, \mathbf{m}))(\mathbf{g}(\mathbf{\Psi_i}, \mathbf{m}) - \bar{\mathbf{g}}(\mathbf{\Psi}, \mathbf{m}))^T, \tag{1}$$

where $\bar{\mathbf{g}}$ is the mean of the ensemble of predictions $\mathbf{g}(\mathbf{\Psi_i}, \mathbf{m})$. In the following, we refer to $\mathbf{C_p}$ estimated in equation (1) as the empirical prediction error covariance matrix. Alternatively, we can compute $\mathbf{C_p}$ following a linearized perturbation approach. We assume that our forward model $\mathbf{g}(\mathbf{\Psi}, \mathbf{m})$ is well approximated by linearized perturbations of our predictions. For an a priori Earth model $\tilde{\mathbf{\Psi}}$ we write:

$$\mathbf{g}(\mathbf{\Psi}, \mathbf{m}) \approx \mathbf{g}(\tilde{\mathbf{\Psi}}, \mathbf{m}) + \mathbf{K_\Psi}(\tilde{\mathbf{\Psi}}, \mathbf{m}) \cdot (\mathbf{\Psi} - \tilde{\mathbf{\Psi}}), \tag{2}$$

where $\mathbf{K_\Psi}(\tilde{\mathbf{\Psi}}, \mathbf{m})$ is the sensitivity kernels of the predictions with respect to elastic parameters used to compute forward predictions:

$$\mathbf{K_\Psi}(\tilde{\mathbf{\Psi}}, \mathbf{m}) = \frac{\partial g_i}{\partial \Psi_j}(\tilde{\mathbf{\Psi}}, \mathbf{m}). \tag{3}$$

In this first order approximation, we use the sensitivity kernel $\mathbf{K_\Psi}(\tilde{\mathbf{\Psi}}, \mathbf{m})$ to estimate the covariance matrix $\mathbf{C_p}$ (Duputel et al., 2014):

$$\mathbf{C_p} = \mathbf{K_\Psi} \cdot \mathbf{C_\Psi} \cdot \mathbf{K_\Psi^T}, \tag{4}$$

where $\mathbf{C_\Psi}$ is the covariance matrix describing uncertainty in the Earth model. To analyze both approaches, we consider a simple test case limited to an uncertain in S-wave velocity

in a single layer (at 30 km depth) using the source parameters of the $M_W = 6.0$ foreshock on 2017-04-23 (see section 3 of the main text). For comparison, we calculate prediction error covariance matrices $\mathbf{C_p}$ using equation (1) and equation (4). We plot in Figure S7 the diagonal components of both matrices for a representative station. We observe that there is an overall good agreement between our first order $\mathbf{C_p}$ and the empirical $\mathbf{C_p}$ matrix. We notice some discrepancies in the variance amplitudes and a time-shift in the late part of the waveforms (after 75s in Figure S7). To explore the origin of these effects, we compare synthetic waveforms predicted from the stochastic models and the waveforms calculated with the first order approach. The results shown in Figure S8 indicate that the time-shift and amplitude difference in Figure S7 are related to the fact that the first order approach is unable to perfectly reproduce large perturbations in the Earth model.

To correct these differences, we can also estimate a covariance matrix using a second order approximation of the forward model as:

$$\mathbf{g}(\mathbf{\Psi}, \mathbf{m}) \approx \mathbf{g}(\tilde{\mathbf{\Psi}}, \mathbf{m}) + \mathbf{K_\Psi}(\tilde{\mathbf{\Psi}}, \mathbf{m}) \cdot (\mathbf{\Psi} - \tilde{\mathbf{\Psi}}) + \frac{1}{2!} (\mathbf{\Psi} - \tilde{\mathbf{\Psi}}) \cdot \mathbf{H_\Psi}(\tilde{\mathbf{\Psi}}, \mathbf{m}) \cdot (\mathbf{\Psi} - \tilde{\mathbf{\Psi}}), \quad (5)$$

where $\mathbf{H}_\Psi$ is the second order derivative with respect to the elastic parameters:

$$\mathbf{H_\Psi}(\tilde{\mathbf{\Psi}}, \mathbf{m}) = \frac{\partial^2 g_i}{\partial \Psi_k \partial \Psi_j}(\tilde{\mathbf{\Psi}}, \mathbf{m}). \quad (6)$$

The computation of H involves evaluating n^2 derivatives, where n is the number of elastic parameters (e.g., 3 parameters per layer for a 1D Earth model). However, assuming that cross-terms are negligible, we can reduce the number of 2nd order derivatives to be evaluated to n.

As shown in Figure S7 and S8, some of the imperfections obtained with the first order approach can be corrected by employing a second order approach neglecting cross-terms.

In practice, these discrepancies are more significant when we apply larger perturbations to the velocity model. Despite the fact that the inaccuracies of the first order approach have been corrected, we notice in Figure S8 that the differences between the first and second order approach are relatively small given the 1 Hz sampling frequency used in our moment tensor inversions. Our tests show that the differences are more visible when inverting waveforms with a higher sampling rate.

References

Altamimi, Z., Rebischung, P., Métivier, L., & Collilieux, X. (2016). ITRF2014: A new release of the International Terrestrial Reference Frame modeling nonlinear station motions. *Journal of Geophysical Research: Solid Earth*, *121*(8), 6109–6131. doi: 10.1002/2016JB013098

Báez, J. C., Leyton, F., Troncoso, C., del Campo, F., Bevis, M., Vigny, C., ... Blume, F. (2018, jul). The Chilean GNSS Network: Current Status and Progress toward Early Warning Applications. *Seismological Research Letters*, *89*(4), 1546–1554. Retrieved from `https://pubs.geoscienceworld.org/ssa/srl/article/89/4/1546/530337/The-Chilean-GNSS-Network-Current-Status-and` doi: 10.1785/0220180011

Duputel, Z., Agram, P. S., Simons, M., Minson, S. E., & Beck, J. L. (2014). Accounting for prediction uncertainty when inferring subsurface fault slip. *Geophysical Journal International*, *197*(1), 464–482.

Nocquet, J. M. (2017). Pyacs: a set of python tools for gps analysis and tectonic modelling. In *Colloque g2.*

Nocquet, J. M., Villegas-Lanza, J. C., Chlieh, M., Mothes, P. A., Rolandone, F., Jarrin, P., ... Yepes, H. (2014). Motion of continental slivers and creeping subduction in the northern Andes. *Nature Geoscience*, *7*(4), 287–291. doi: 10.1038/ngeo2099

Piñón, D. A., Gómez, D. D., Smalley, R., Cimbaro, S. R., Lauría, E. A., & Bevis, M. G. (2018, mar). The History, State, and Future of the Argentine Continuous Satellite Monitoring Network and Its Contributions to Geodesy in Latin America. *Seismological Research Letters*, *89*(2A), 475–482. Retrieved from `https://pubs.geoscienceworld.org/ssa/srl/article/89/2A/475/528199/The-History-State-and-Future-of-the-Argentine` doi: 10.1785/0220170162

Ruiz, J. A., Contreras-Reyes, E., Ortega-Culaciati, F., & Manríquez, P. (2018). Rupture process of the april 24, 2017, mw 6.9 valparaíso earthquake from the joint inversion of teleseismic body waves and near-field data. *Physics of the Earth and Planetary Interiors*, *279*, 1–14.

Ruiz, S., Aden-Antoniow, F., Baez, J., Otarola, C., Potin, B., del Campo, F., ... others (2017). Nucleation phase and dynamic inversion of the mw 6.9 valparaíso 2017 earthquake in central chile. *Geophysical Research Letters*, *44*(20), 10–290.

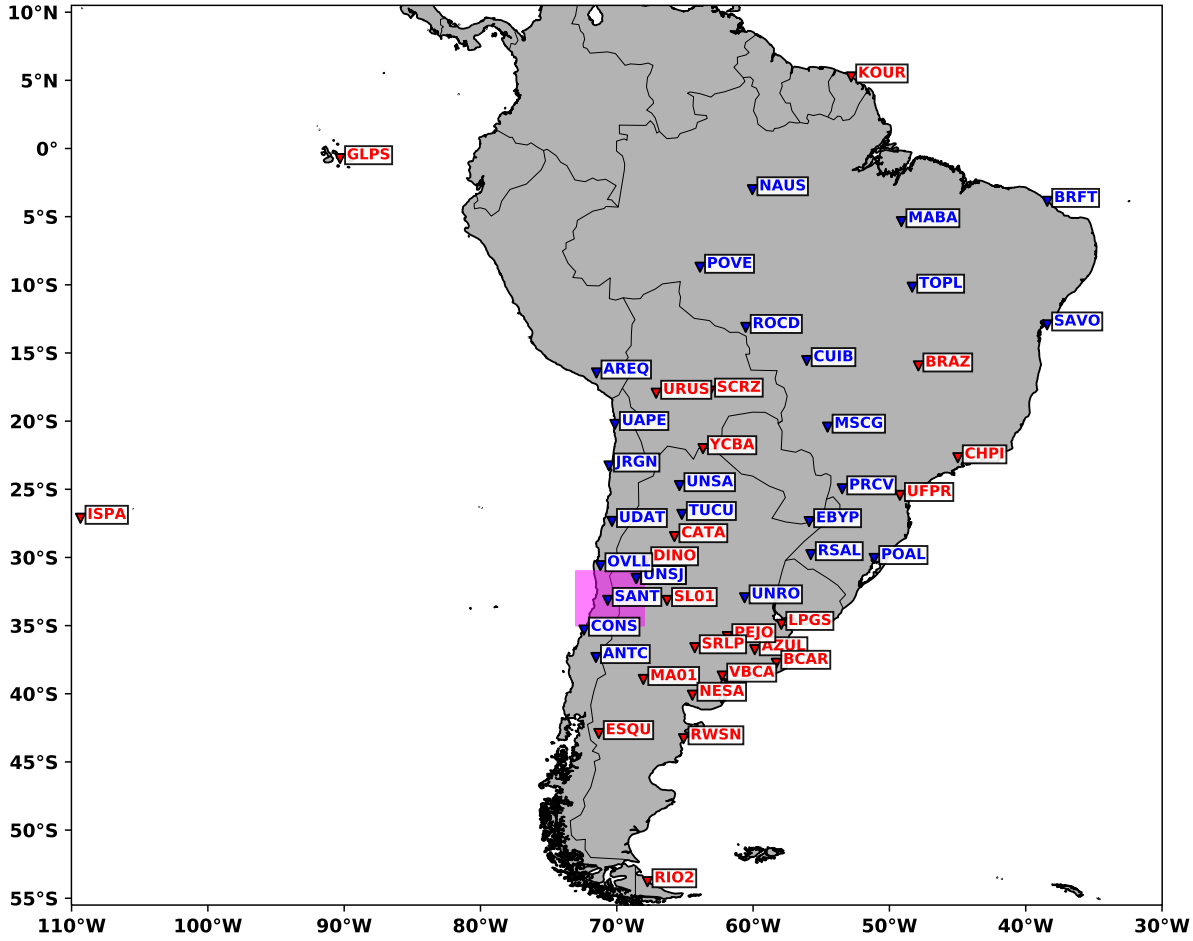

Figure S1. Map of the GPS stations processed in South America and Nazca Plates. The red stations are those ones used to define the Reference Frame, while the blue ones are just used on the processing. The pink box denotes the study area (see Figure S2 to look at the stations processed in this region).

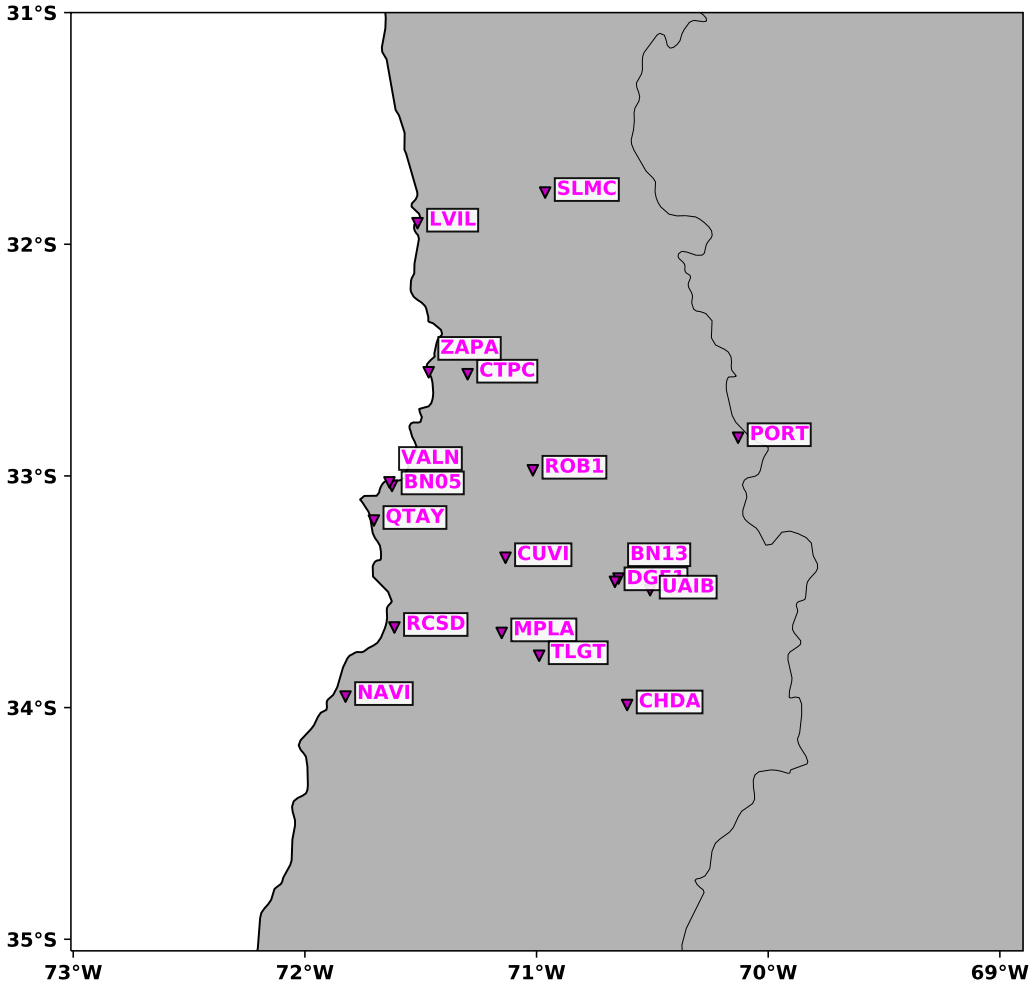

Figure S2. Map of the GPS stations processed in the study area.

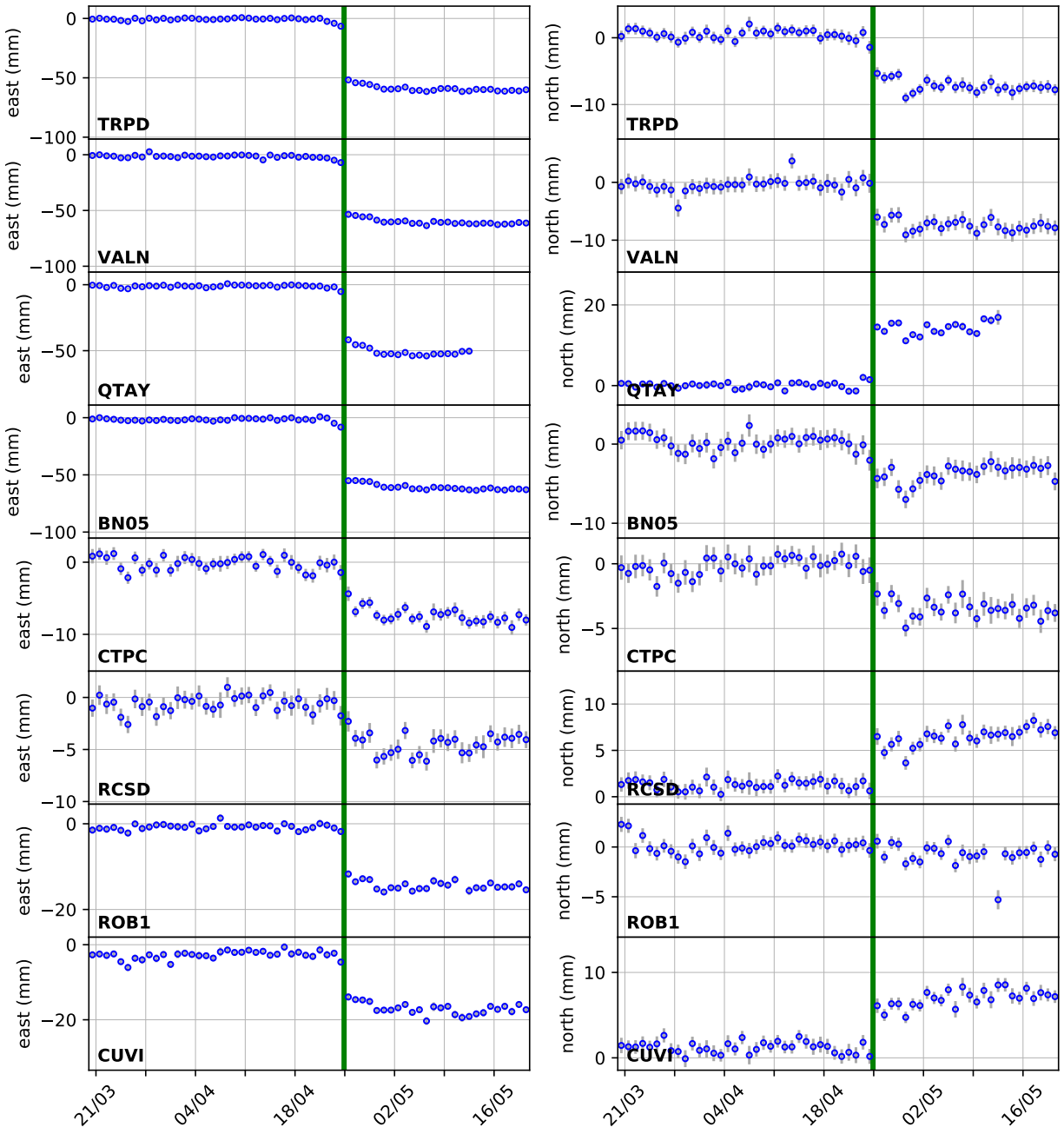

Figure S3. GPS time series for the Valparaíso region network for north and east component. The images show the time series before and after the mainshock (green line) of the sequence.

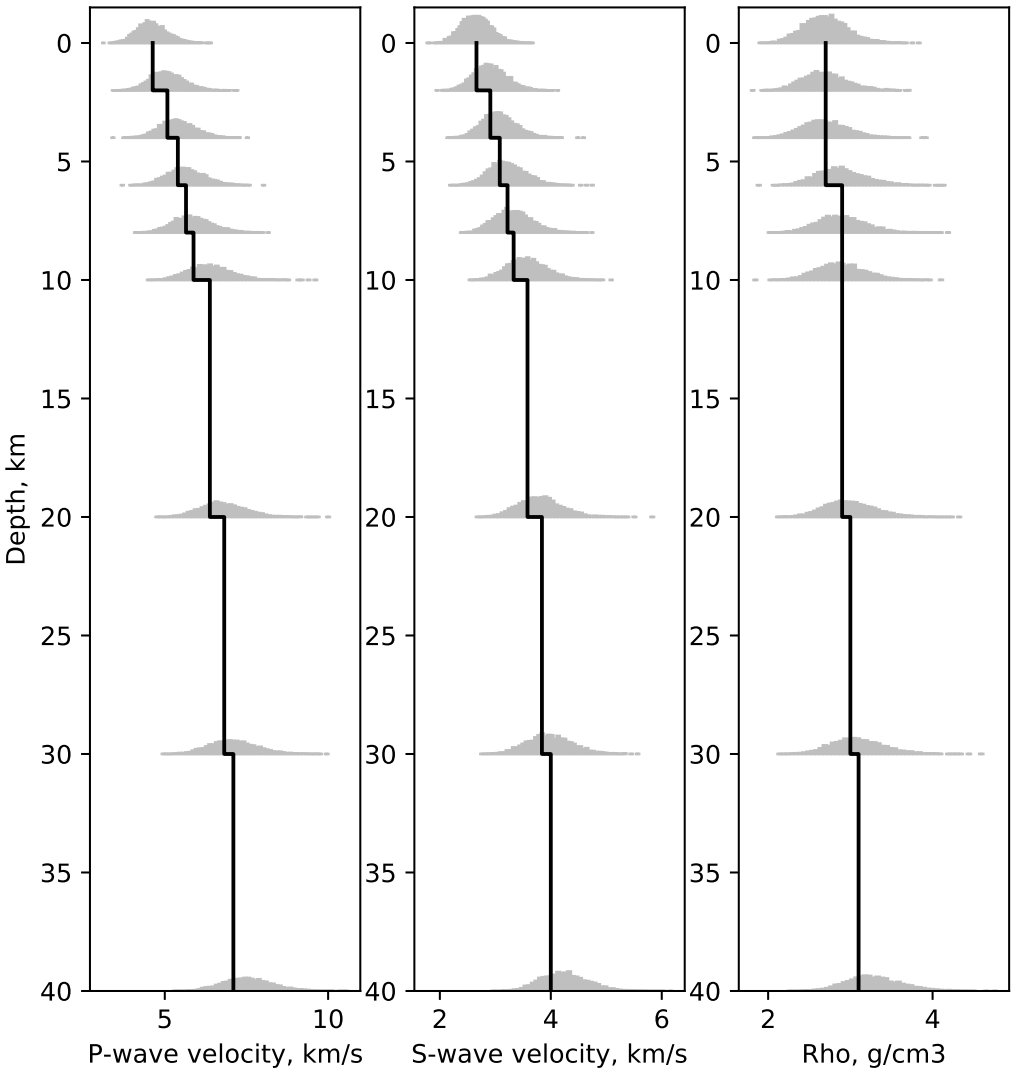

Figure S4. Model variability of the P-wave, S-wave, and density as a function of depth in Valparaíso region. Black line represents the velocity layered model used for Green's Function (GF) calculation. Grey histograms are the probability density function for each parameter as a function of depth as described in Cp.

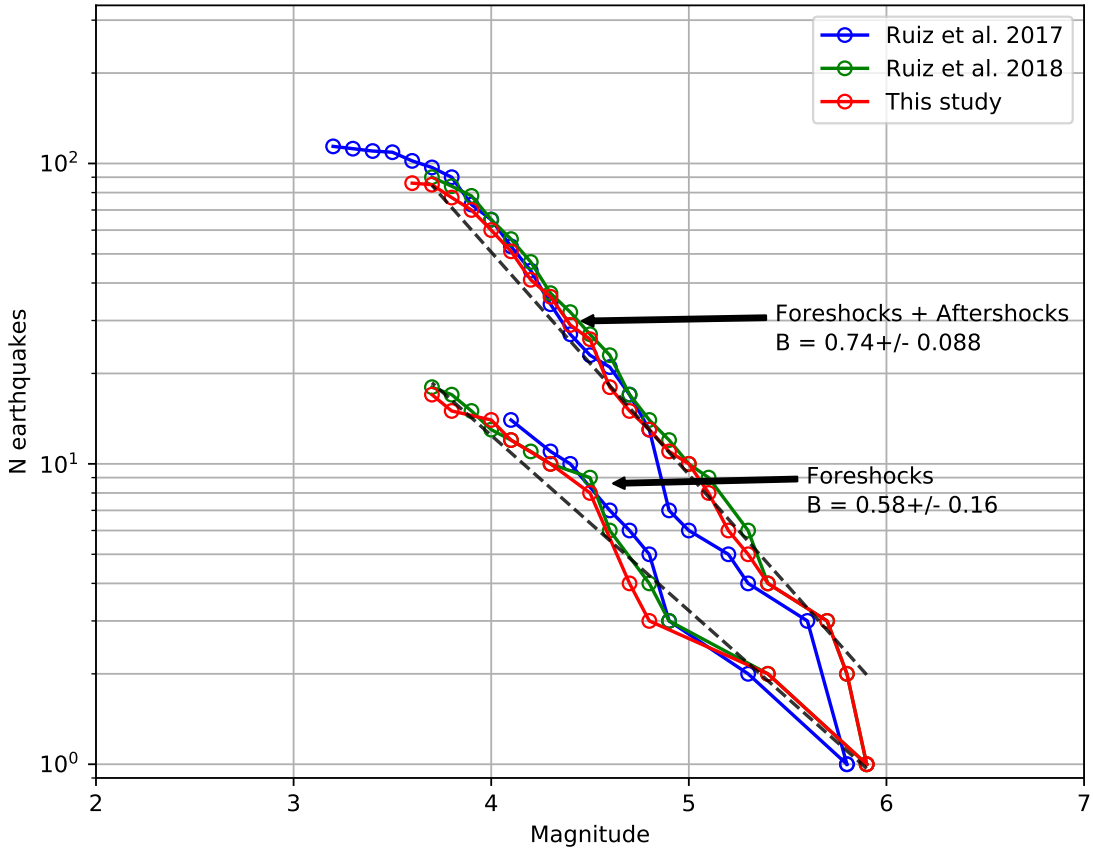

Figure S5. Gutenberg-Richter law for the 2017 Valparaíso earthquake sequence. Three different catalogs of the sequence are shown: Our CMT catalog, S. Ruiz et al. (2017) catalog, and J. A. Ruiz et al. (2018) catalog. For each catalog, both the whole sequence (foreshocks and aftershocks), and the foreshocks sequence are represented.

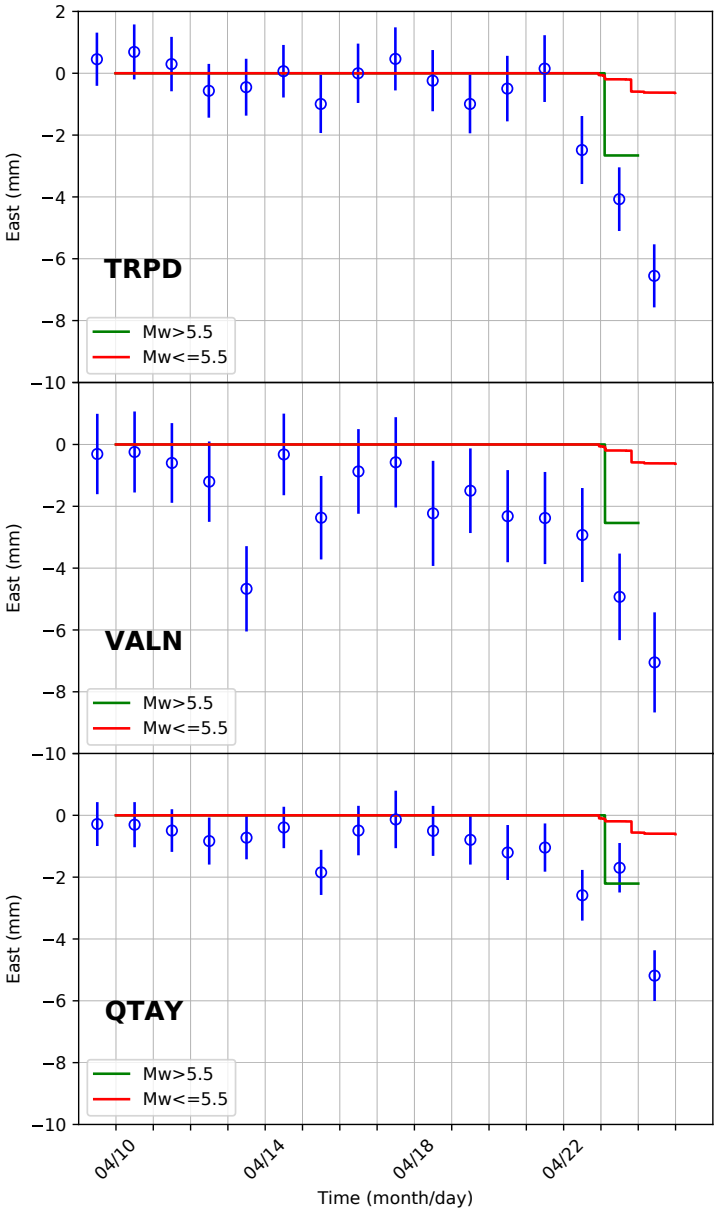

Figure S6. Synthetic surface displacement for different ranges of magnitude, foreshocks with $M_w \geq 5.5$ (largest foreshock $M_w = 6.0$) and foreshocks with $M_w \leq 5.5$. The $M_w = 6.0$ contribution appears to dominate the signal, with respect to the cumulative contribution of smaller foreshocks.

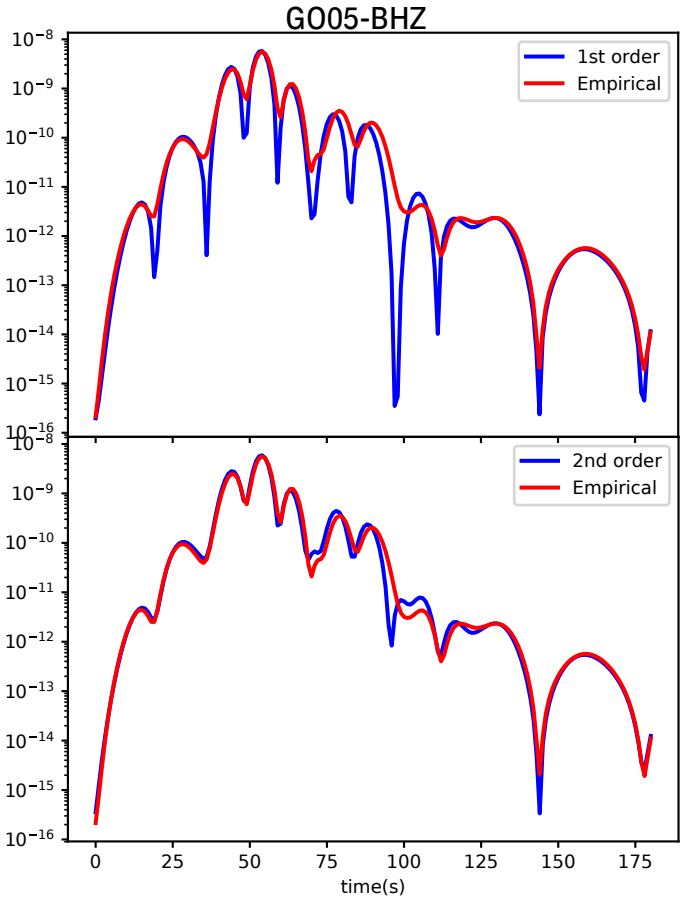

Figure S7. Diagonal of the $\mathbf{C_p}$ matrix for the vertical component of the station G005. The matrix is calculated for the $M_W = 6.0$ foreshock of the Valparaíso sequence (see section 3 of the main text). The red line represents the diagonal matrix for the empirical covariance matrix (i.e., the matrix created from an ensemble of models). The blue line represents the first (top) and second-order (bottom) approaches used to compute $\mathbf{C_p}$.

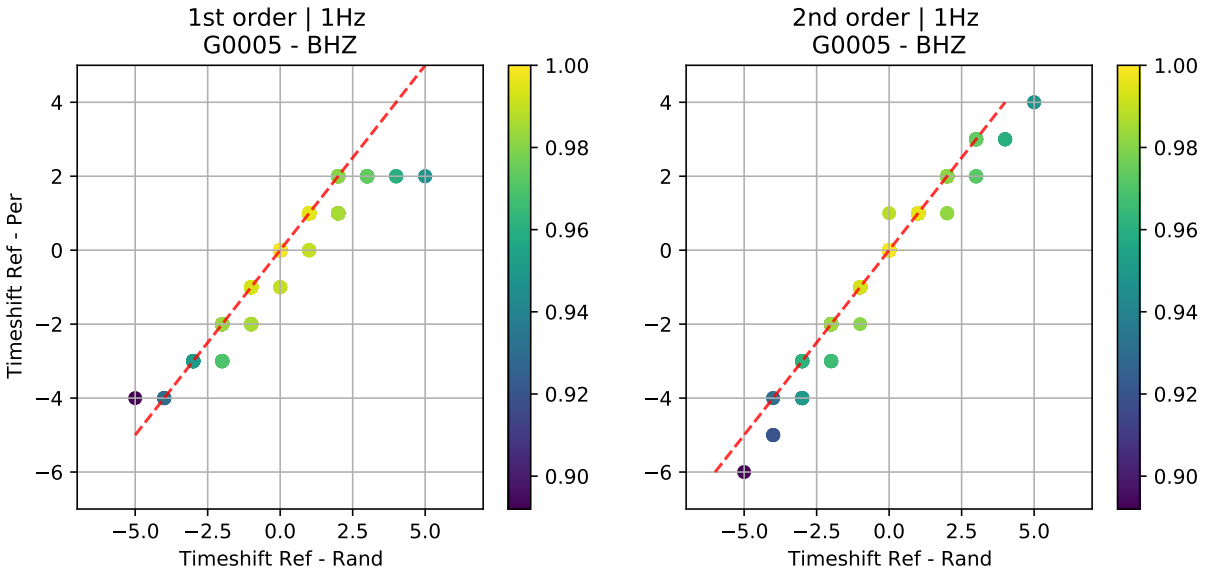

Figure S8. Comparison between synthetic waveforms predicted from stochastic models calculated with a log-normal distribution, and synthetic waveforms calculated using the first and second order $\mathbf{C_p}$ matrix. The waveforms are generated using the source model of the $M_W = 6.0$ foreshock presented in section 3 of the main text. The X-axis represents time shifts between waveforms generated with the average velocity model of the region (figure S4) and waveform predicted for randomly perturbed velocity models. The Y-axis represents time shifts between waveforms generated with the average velocity model and waveforms generated either with the first or the second order approximation (see equations (2) and (5) of text S2). The color represents the correlation coefficient of each pair of waveforms. If the comparison follows the $y = x$ line, it means that the perturbation approximation properly estimates the empirical covariance matrix. We can observe that the second order approach better approximates actual synthetics (especially when there is a significant time-delay between waveforms).

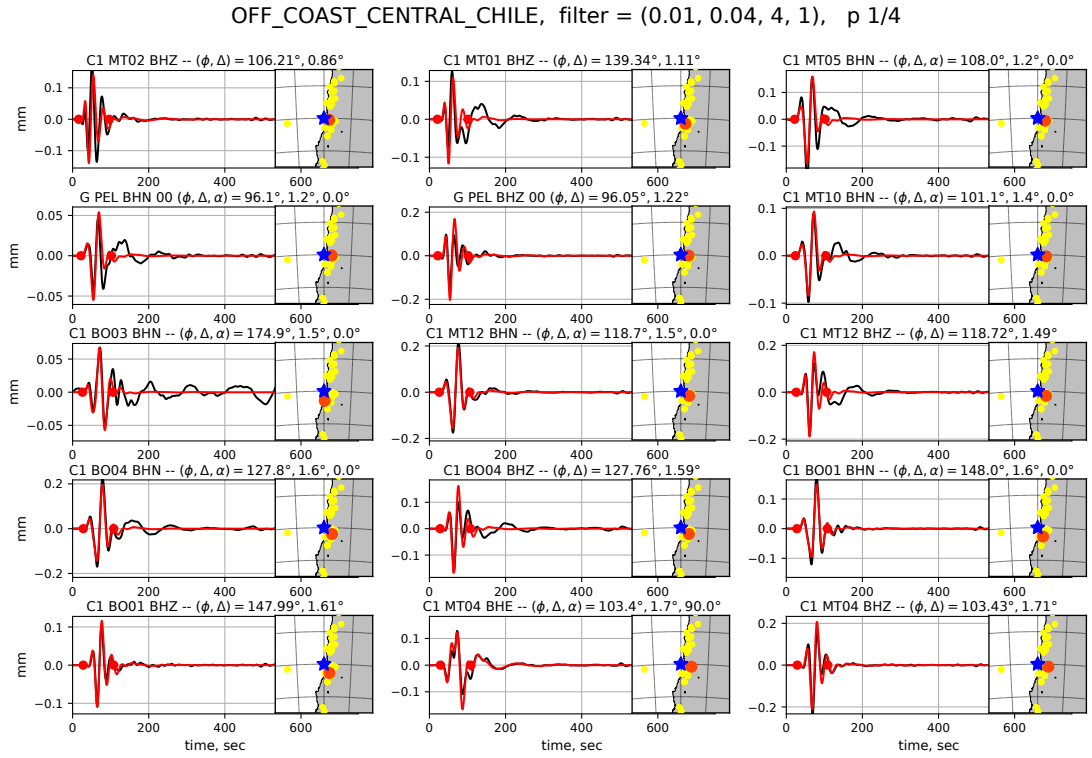
OFF_COAST_CENTRAL_CHILE, filter = (0.01, 0.04, 4, 1), p 1/4
C1 MT02 BHZ -- (ϕ, Δ) = 106.21°, 0.86°
C1 MT01 BHZ -- (ϕ, Δ) = 139.34°, 1.11°
C1 MT05 BHN -- (ϕ, Δ, α) = 108.0°, 1.2°, 0.0°
G PEL BHN 00 (ϕ, Δ, α) = 96.1°, 1.2°, 0.0°
G PEL BHZ 00 (ϕ, Δ) = 96.05°, 1.22°
C1 MT10 BHN -- (ϕ, Δ, α) = 101.1°, 1.4°, 0.0°
C1 BO03 BHN -- (ϕ, Δ, α) = 174.9°, 1.5°, 0.0°
C1 MT12 BHN -- (ϕ, Δ, α) = 118.7°, 1.5°, 0.0°
C1 MT12 BHZ -- (ϕ, Δ) = 118.72°, 1.49°
C1 BO04 BHN -- (ϕ, Δ, α) = 127.8°, 1.6°, 0.0°
C1 BO04 BHZ -- (ϕ, Δ) = 127.76°, 1.59°
C1 BO01 BHN -- (ϕ, Δ, α) = 148.0°, 1.6°, 0.0°
C1 BO01 BHZ -- (ϕ, Δ) = 147.99°, 1.61°
C1 MT04 BHE -- (ϕ, Δ, α) = 103.4°, 1.7°, 90.0°
C1 MT04 BHZ -- (ϕ, Δ) = 103.43°, 1.71°
mm
time, sec

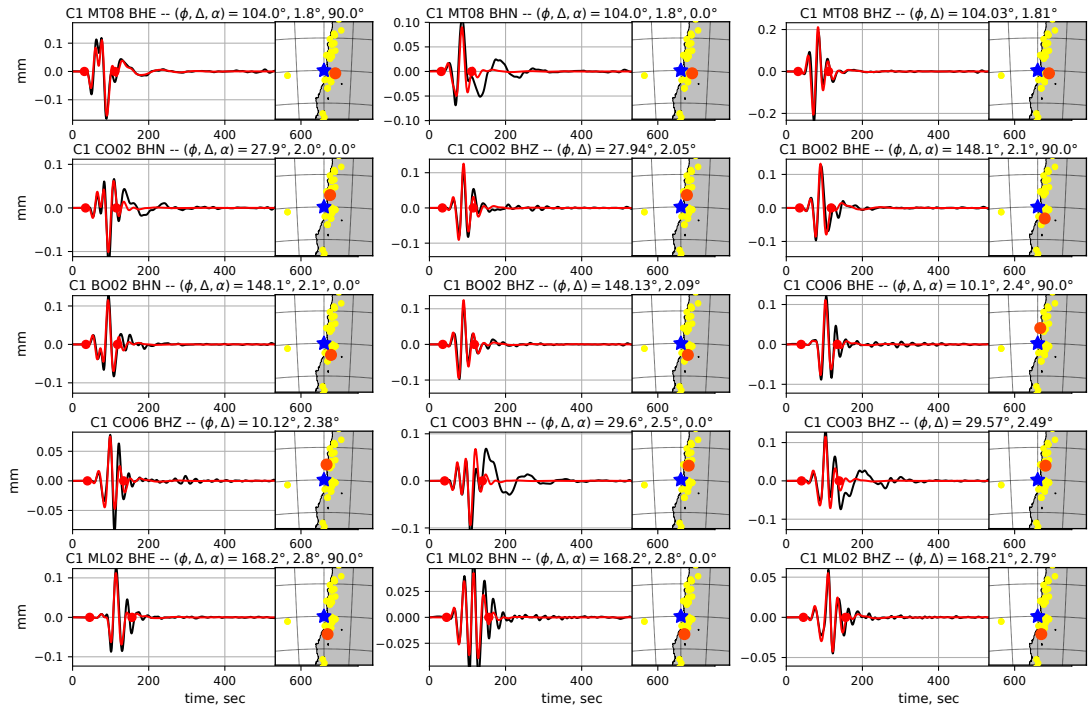
OFF_COAST_CENTRAL_CHILE, filter = (0.01, 0.04, 4, 1), p 2/4
C1 MT08 BHE -- (ϕ, Δ, α) = 104.0°, 1.8°, 90.0°
C1 MT08 BHN -- (ϕ, Δ, α) = 104.0°, 1.8°, 0.0°
C1 MT08 BHZ -- (ϕ, Δ) = 104.03°, 1.81°
C1 CO02 BHN -- (ϕ, Δ, α) = 27.9°, 2.0°, 0.0°
C1 CO02 BHZ -- (ϕ, Δ) = 27.94°, 2.05°
C1 BO02 BHE -- (ϕ, Δ, α) = 148.1°, 2.1°, 90.0°
C1 BO02 BHN -- (ϕ, Δ, α) = 148.1°, 2.1°, 0.0°
C1 BO02 BHZ -- (ϕ, Δ) = 148.13°, 2.09°
C1 CO06 BHE -- (ϕ, Δ, α) = 10.1°, 2.4°, 90.0°
C1 CO06 BHZ -- (ϕ, Δ) = 10.12°, 2.38°
C1 CO03 BHN -- (ϕ, Δ, α) = 29.6°, 2.5°, 0.0°
C1 CO03 BHZ -- (ϕ, Δ) = 29.57°, 2.49°
C1 ML02 BHE -- (ϕ, Δ, α) = 168.2°, 2.8°, 90.0°
C1 ML02 BHN -- (ϕ, Δ, α) = 168.2°, 2.8°, 0.0°
C1 ML02 BHZ -- (ϕ, Δ) = 168.21°, 2.79°
mm
time, sec

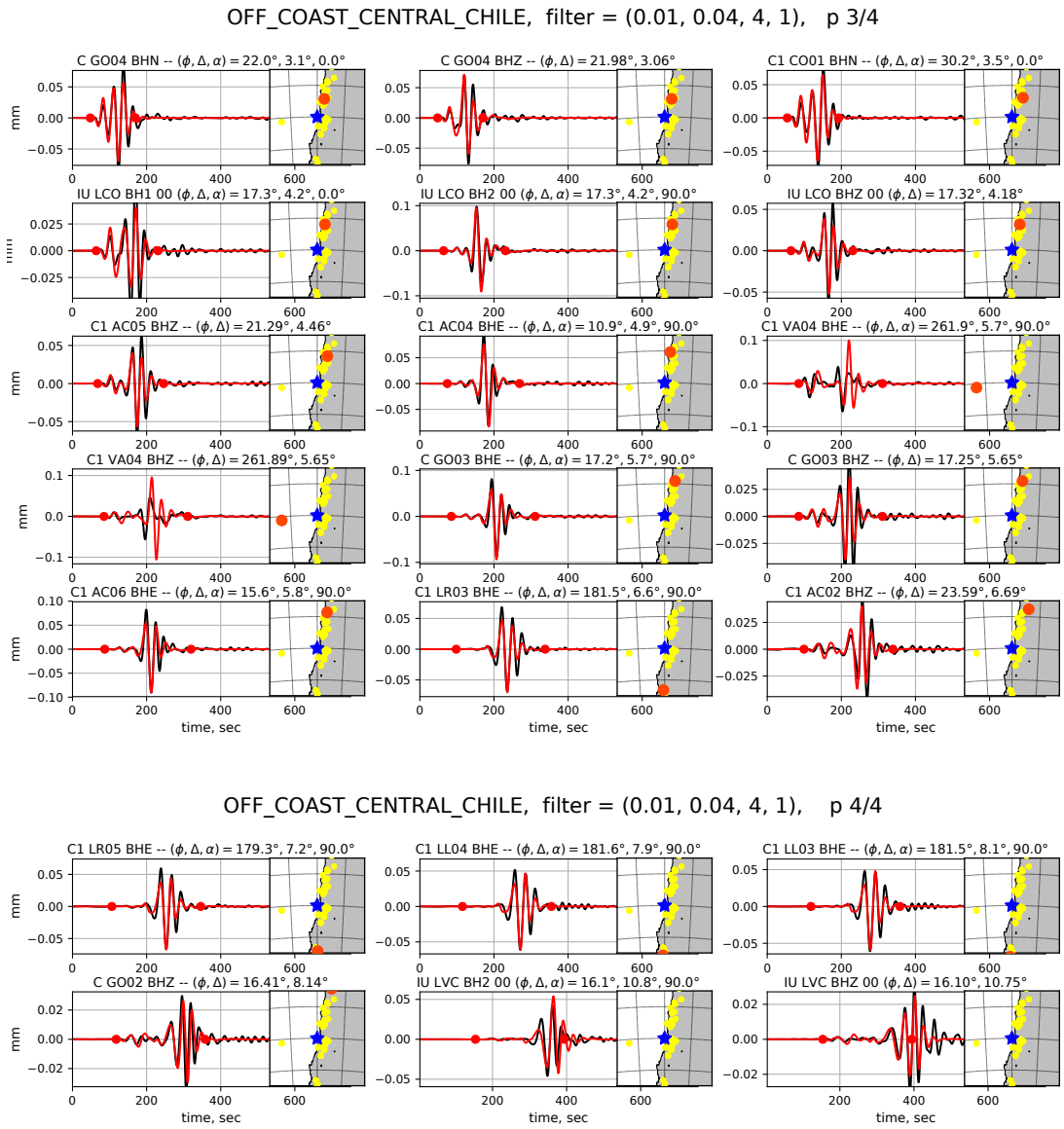

Figure S9. Waveforms fit for the $M_W = 6.0$ foreshock using CMT solution from our catalog. Observed (black) and synthetic (red) waveforms for a given station (orange). The fit (inversion) is made between red dots. The blue star represents the CMT location. Yellow dots correspond to the ensemble of stations used in the inversion.

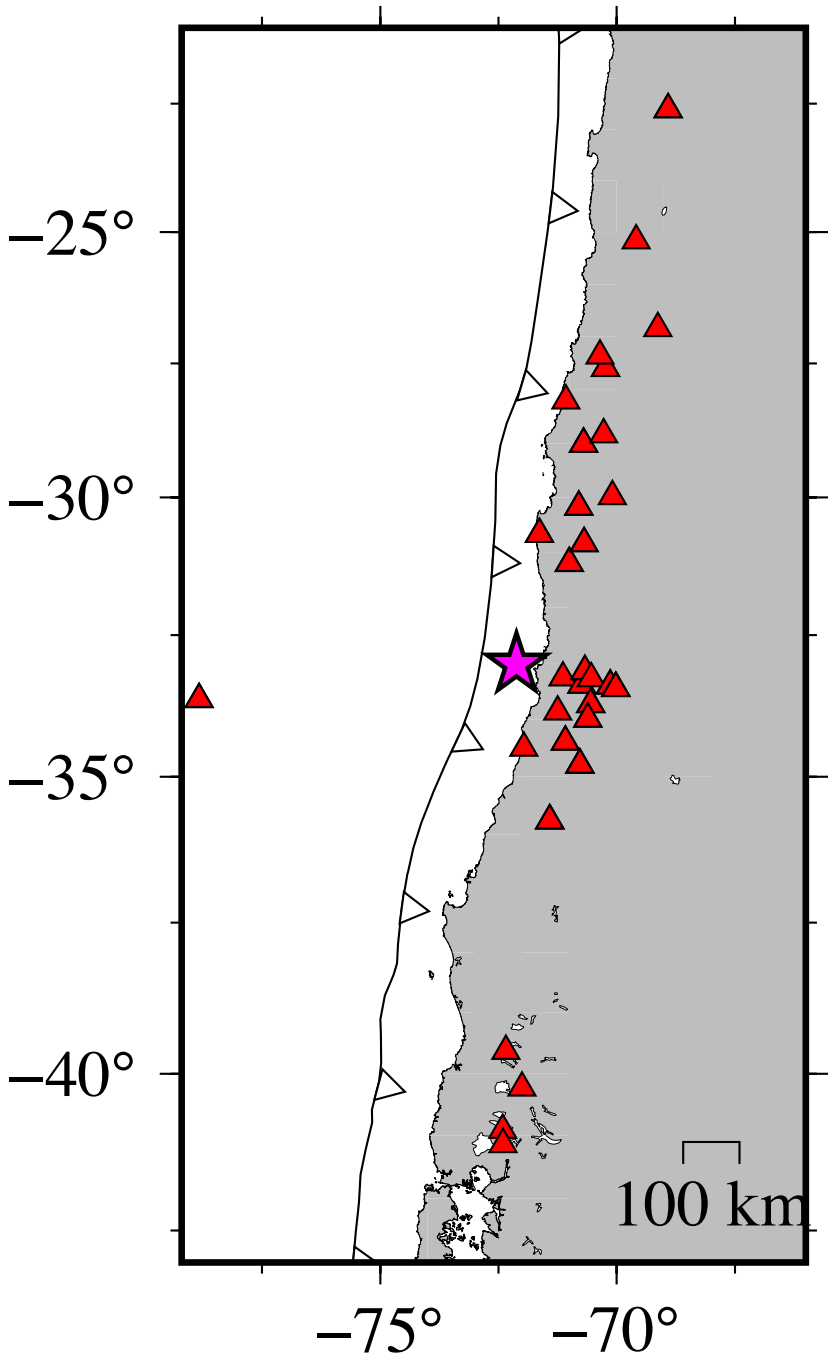

Figure S10. Stations used for the $M_W = 6$ foreshock CMT inversion. The CMT location is shown in purple.

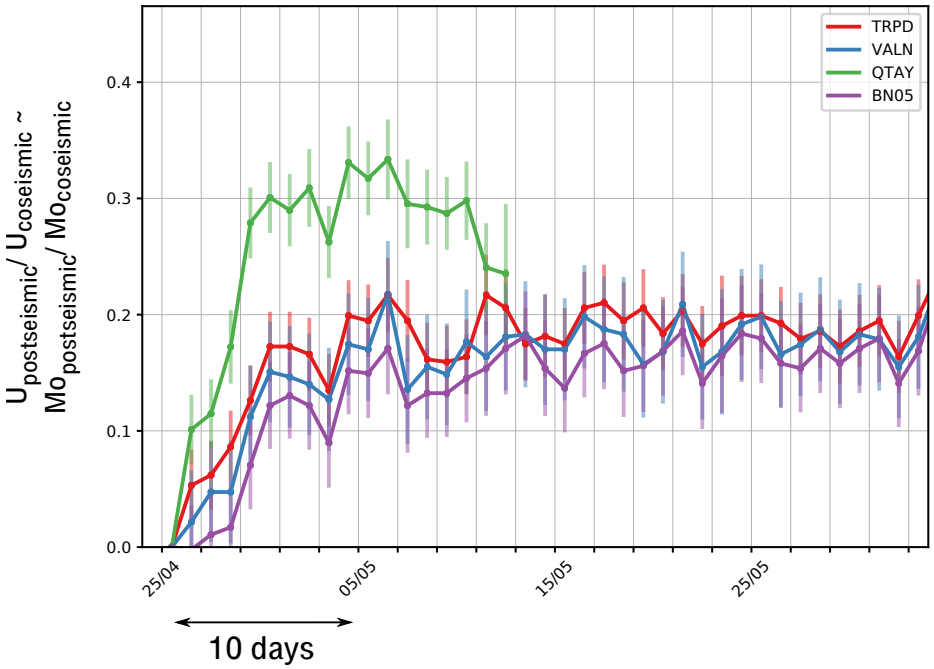

Figure S11. Mainshock postseismic surface displacement normalized by the coseismic displacement at each GPS station. This ratio approximates the moment ratio between postseismic and coseismic terms.

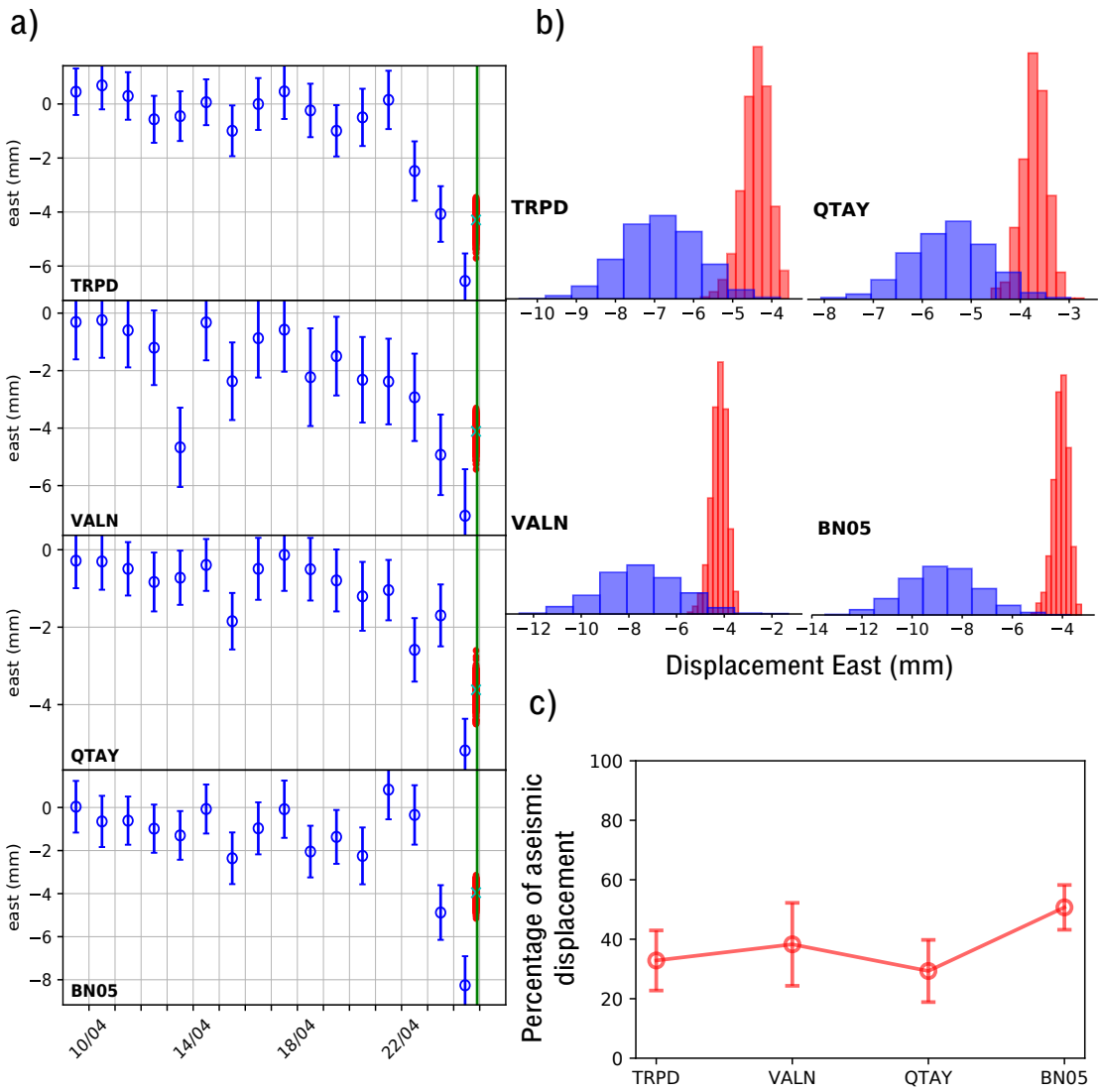

Figure S12. Same as Figure 4 of main text but with the quick postseismic contribution produced by the largest foreshock.

Table S1. Bandpass filter corner frequencies used for CMT inversion

Magnitude	Low Corner Freq (Hz)	High Corner Freq (Hz)
< 4.5	0.02	0.08
> 4.5	0.015	0.06
6.0	0.01	0.04

Table S2: CMT solutions of our catalog.

Date	Time	Lon °	Lat °	Depth km	M0 N·m	Mw	Mrr N·m	Mtt N·m	Mpp N·m	Mrt N·m	Mrp N·m	Mtp N·m
2017-04-15	01:50:23	-70.85	-31.93	35.5	3.56e+14	3.63	-1.49e+20	-8.60e+20	1.01e+21	-1.82e+20	-1.83e+21	2.927e+21
2017-04-22	22:46:44	-71.96	-33.14	17.5	2.21e+16	4.83	1.76e+23	-1.58e+22	-1.60e+23	-2.78e+22	-1.41e+23	3.324e+21
2017-04-22	23:57:13	-72.03	-33.05	21.5	2.10e+15	4.15	1.28e+22	-1.07e+21	-1.17e+22	-8.45e+20	-1.70e+22	9.225e+20
2017-04-23	01:49:12	-72.06	-33.03	22.5	8.47e+15	4.55	5.58e+22	2.57e+21	-5.83e+22	-5.42e+21	-6.24e+22	9.259e+20
2017-04-23	02:36:06	-72.10	-33.03	19.5	1.16e+18	6.0	7.45e+24	-3.96e+23	-7.05e+24	4.10e+23	-9.06e+24	-5.981e+22
2017-04-23	02:43:18	-71.89	-33.05	21.5	1.76e+16	4.76	7.84e+22	2.41e+22	-1.03e+23	-1.86e+22	-1.44e+23	-4.994e+22
2017-04-23	02:52:38	-72.00	-33.05	25.5	8.02e+15	4.54	6.41e+22	-5.19e+20	-6.36e+22	1.29e+21	-4.66e+22	-1.311e+22
2017-04-23	03:00:12	-71.97	-32.86	14.5	5.04e+15	4.40	3.97e+22	-7.83e+21	-3.19e+22	-9.10e+21	-3.43e+22	4.470e+21
2017-04-23	03:02:17	-72.02	-33.07	26.5	8.48e+15	4.55	7.48e+22	-5.13e+21	-6.97e+22	6.45e+21	-4.39e+22	-2.778e+21
2017-04-23	12:52:15	-71.99	-33.07	26.5	5.42e+14	3.76	3.07e+21	2.78e+20	-3.34e+21	4.33e+20	-4.30e+21	-6.063e+20
2017-04-23	16:12:54	-71.96	-32.99	25.5	1.93e+15	4.12	1.12e+22	-2.14e+21	-9.07e+21	-7.36e+20	-1.63e+22	-9.098e+20
2017-04-23	19:40:10	-72.16	-33.05	21.5	2.10e+17	5.5	1.69e+24	-1.06e+23	-1.59e+24	5.75e+22	-1.31e+24	8.445e+22
2017-04-23	20:30:50	-72.10	-33.06	30.5	1.50e+15	4.05	5.58e+21	1.06e+22	-1.62e+22	2.95e+21	-5.86e+21	-3.027e+20
2017-04-24	01:19:42	-72.04	-33.11	22.5	1.31e+15	4.01	6.16e+21	9.72e+20	-7.14e+21	4.68e+20	-1.12e+22	-1.181e+21
2017-04-24	03:50:50	-72.14	-33.09	24.5	4.53e+15	4.37	3.42e+22	-3.71e+21	-3.05e+22	3.65e+21	-3.11e+22	4:655e+21
2017-04-24	03:54:11	-72.05	-33.10	21.5	7.87e+15	4.53	5.58e+22	-2.75e+21	-5.30e+22	8.92e+21	-5.55e+22	-8.387e+21
2017-04-24	06:54:36	-72.06	-33.11	23.5	7.69e+14	3.86	4.85e+21	-7.75e+20	-4.07e+21	1.17e+21	-6.13e+21	4.638e+20
2017-04-24	13:17:02	-71.93	-33.00	28.5	5.03e+14	3.73	2.19e+21	1.04e+21	-3.23e+21	-7.60e+18	-4.09e+21	-1.127e+21
2017-04-24	23:54:45	-71.93	-33.29	35.5	1.43e+16	4.70	5.65e+22	3.38e+22	-9.04e+22	2.77e+22	-1.16e+23	-1.953e+22
2017-04-25	00:17:36	-72.04	-33.17	20.5	7.58e+15	4.52	6.05e+22	-5.41e+21	-5.51e+22	-5.64e+21	-4.85e+22	5.282e+21
2017-04-25	01:33:15	-72.04	-33.16	22.5	1.56e+16	4.73	1.27e+23	-3.88e+21	-1.23e+23	1.73e+22	-9.06e+22	6.894e+21
2017-04-25	01:43:03	-72.09	-33.16	22.5	6.78e+16	5.15	5.20e+23	-3.77e+22	-4.82e+23	2.10e+22	-4.56e+23	5.773e+21
2017-04-25	01:54:30	-72.11	-33.10	22.5	1.45e+15	4.04	2.60e+21	2.37e+21	-4.97e+21	8.85e+20	-1.22e+22	-6.659e+21
2017-04-25	02:33:05	-71.89	-33.00	32.5	9.88e+14	3.93	8.24e+21	-2.88e+21	-5.36e+21	1.11e+21	-7.10e+21	-3.851e+20
2017-04-25	03:02:23	-72.08	-33.16	23.5	9.33e+15	4.58	7.71e+22	-1.13e+22	-6.58e+22	8.15e+21	-5.93e+22	3.680e+21
2017-04-25	05:56:26	-72.28	-33.03	17.5	2.43e+15	4.19	2.26e+22	-5.64e+21	-1.70e+22	-6.61e+19	-1.27e+22	4.963e+21
2017-04-25	06:34:15	-71.93	-32.97	25.5	4.88e+14	3.73	3.60e+21	-5.02e+20	-3.10e+21	-6.10e+20	-3.50e+21	4.637e+19
2017-04-25	08:15:17	-71.98	-32.97	24.5	9.43e+14	3.92	5.98e+21	-5.54e+20	-5.43e+21	1.41e+20	-7.48e+21	-6.557e+20
2017-04-25	08:29:06	-72.09	-33.15	19.5	1.21e+15	3.99	8.03e+21	7.54e+20	-8.78e+21	3.61e+20	-8.67e+21	-1.002e+20
2017-04-25	09:33:31	-72.00	-33.10	27.5	3.85e+15	4.32	2.18e+22	-3.06e+21	-1.87e+22	5.88e+21	-3.20e+22	-3.549e+21
2017-04-25	10:20:23	-72.11	-32.92	21.5	1.95e+15	4.13	8.25e+21	-2.08e+20	-8.04e+21	-1.85e+21	-1.76e+22	-2.089e+20

Continued on next page

Table S2 – *Continued from previous page*

Date	Time	Lon °	Lat °	Depth km	M0 N·m	Mw	Mrr N·m	Mtt N·m	Mpp N·m	Mrt N·m	Mrp N·m	Mtp N·m
2017-04-25	10:24:35	-72.14	-32.90	22.5	2.28e+15	4.17	1.90e+22	-2.81e+21	-1.62e+22	-1.29e+21	-1.43e+22	-2.237e+21
2017-04-25	11:22:02	-72.20	-33.03	19.5	1.03e+15	3.94	8.45e+21	-1.21e+21	-7.24e+21	3.36e+19	-6.50e+21	1.057e+21
2017-04-25	11:24:09	-72.27	-33.12	19.5	1.70e+15	4.09	1.50e+22	-2.19e+21	-1.28e+22	3.35e+21	-9.24e+21	2.462e+20
2017-04-25	12:13:23	-72.21	-33.12	19.5	1.21e+16	4.65	1.02e+23	-1.01e+22	-9.21e+22	1.81e+22	-6.92e+22	2.311e+21
2017-04-25	12:37:37	-72.16	-33.05	21.5	1.31e+15	4.01	8.31e+21	-3.74e+20	-7.94e+21	1.08e+20	-1.02e+22	1.217e+21
2017-04-25	14:26:35	-72.10	-33.17	21.5	2.76e+15	4.23	1.34e+22	7.15e+20	-1.41e+22	2.13e+21	-2.37e+22	2.934e+21
2017-04-25	15:32:07	-72.21	-33.10	19.5	1.18e+15	3.98	1.15e+22	-2.05e+21	-9.41e+21	-5.21e+20	-4.93e+21	2.174e+21
2017-04-25	16:38:53	-72.18	-33.07	19.5	1.41e+15	4.03	9.02e+21	4.71e+20	-9.49e+21	4.63e+20	-1.06e+22	-5.471e+20
2017-04-25	16:48:36	-72.01	-33.31	24.5	1.99e+15	4.13	9.15e+21	6.87e+20	-9.84e+21	7.19e+21	-1.58e+22	1.966e+21
2017-04-25	20:57:54	-72.15	-33.13	19.5	1.16e+15	3.98	9.76e+21	-9.29e+20	-8.83e+21	1.11e+21	-6.90e+21	-3.074e+19
2017-04-25	21:03:13	-72.06	-33.12	17.5	8.67e+14	3.89	6.93e+21	-2.24e+21	-4.69e+21	1.96e+21	-6.05e+21	6.534e+20
2017-04-25	23:58:11	-71.98	-32.95	26.5	1.25e+15	4.00	1.04e+22	-1.85e+21	-8.51e+21	1.59e+20	-8.10e+21	1.225e+21
2017-04-26	00:43:00	-71.96	-32.94	26.5	4.63e+14	3.71	1.77e+21	2.60e+20	-2.03e+21	-4.96e+20	-4.19e+21	-5.287e+19
2017-04-26	10:05:34	-72.21	-33.14	21.5	4.05e+15	4.34	3.21e+22	-3.83e+21	-2.82e+22	6.22e+21	-2.64e+22	1.765e+20
2017-04-26	14:45:55	-71.85	-33.29	27.5	4.49e+15	4.37	3.33e+22	-2.38e+20	-3.31e+22	3.36e+21	-3.00e+22	1.143e+21
2017-04-26	15:14:01	-71.99	-33.30	31.5	4.64e+15	4.38	3.80e+22	7.82e+20	-3.88e+22	9.17e+21	-2.42e+22	2.401e+21
2017-04-27	01:55:05	-71.81	-33.13	32.5	1.05e+15	3.95	9.92e+21	-3.26e+20	-9.59e+21	9.98e+20	-3.61e+21	1.043e+21
2017-04-27	05:09:22	-71.90	-33.31	27.5	4.06e+16	5.01	3.31e+23	1.23e+22	-3.43e+23	8.57e+21	-2.13e+23	7.488e+22
2017-04-27	06:55:45	-71.88	-33.29	25.5	1.86e+15	4.11	1.23e+22	-7.08e+20	-1.16e+22	1.08e+21	-1.42e+22	-1.304e+20
2017-04-27	08:24:41	-71.89	-33.28	28.5	1.34e+16	4.68	1.04e+23	7.86e+21	-1.12e+23	6.07e+21	-7.88e+22	3.411e+21
2017-04-27	08:46:34	-72.06	-33.10	23.5	1.70e+15	4.09	8.60e+21	-5.83e+20	-8.01e+21	1.44e+21	-1.47e+22	-4.253e+20
2017-04-27	21:17:33	-71.92	-33.30	29.5	8.93e+14	3.90	5.29e+21	1.21e+21	-6.50e+21	2.02e+20	-6.69e+21	-4.765e+20
2017-04-28	15:30:05	-72.02	-33.26	23.5	7.43e+17	5.85	5.32e+24	-2.17e+23	-5.10e+24	1.60e+24	-5.03e+24	5.323e+23
2017-04-28	15:33:30	-71.96	-33.32	23.5	2.32e+16	4.84	1.72e+23	-1.56e+22	-1.57e+23	4.19e+22	-1.58e+23	-1.243e+22
2017-04-28	15:40:24	-71.91	-33.26	28.5	8.66e+15	4.56	4.40e+22	1.25e+22	-5.65e+22	4.84e+22	-4.91e+22	-2.064e+22
2017-04-28	15:49:44	-71.91	-33.31	26.5	2.89e+16	4.91	1.74e+23	2.36e+22	-1.98e+23	3.56e+22	-2.18e+23	1.129e+22
2017-04-28	15:58:34	-72.05	-33.26	27.5	1.32e+17	5.35	9.24e+23	-2.51e+22	-8.98e+23	3.88e+23	-8.39e+23	2.300e+23
2017-04-28	16:05:57	-71.66	-33.17	29.5	5.06e+17	5.74	3.37e+24	-4.38e+23	-2.93e+24	-6.71e+23	-3.88e+24	5.465e+23
2017-04-28	17:09:40	-71.93	-33.25	20.5	7.87e+15	4.53	2.26e+22	1.64e+22	-3.91e+22	2.52e+22	-6.67e+22	-3.073e+21
2017-04-28	17:21:48	-72.06	-33.23	24.5	3.25e+15	4.27	1.51e+22	2.05e+21	-1.72e+22	9.80e+21	-2.64e+22	-6.374e+19
2017-04-28	17:38:09	-71.93	-33.35	29.5	4.21e+15	4.35	-1.54e+22	-8.40e+21	2.38e+22	2.62e+22	-8.34e+21	-2.420e+22
2017-04-28	17:41:50	-71.98	-33.30	25.5	1.11e+17	5.30	7.98e+23	-2.82e+22	-7.70e+23	2.17e+21	-7.79e+23	-3.052e+22

Continued on next page

Table S2 – *Continued from previous page*

Date	Time	Lon °	Lat °	Depth km	M0 N·m	Mw	Mrr N·m	Mtt N·m	Mpp N·m	Mrt N·m	Mrp N·m	Mtp N·m
2017-04-28	17:57:07	-71.94	-33.36	30.5	2.57e+15	4.21	1.60e+22	1.97e+21	-1.79e+22	-3.88e+21	-1.88e+22	3.429e+20
2017-04-28	18:28:23	-71.96	-33.28	29.5	2.68e+15	4.22	1.30e+22	9.66e+20	-1.39e+22	3.90e+21	-2.28e+22	-1.247e+21
2017-04-29	01:06:23	-72.02	-33.25	20.5	4.87e+14	3.73	1.49e+21	1.13e+21	-2.63e+21	2.44e+21	-3.40e+21	-1.148e+21
2017-04-29	01:08:35	-71.99	-33.37	27.5	5.34e+15	4.42	3.22e+22	2.74e+21	-3.49e+22	-3.80e+21	-4.03e+22	-9.976e+21
2017-04-29	01:37:16	-72.07	-33.23	25.5	5.16e+15	4.41	3.27e+22	4.71e+21	-3.74e+22	2.14e+22	-3.01e+22	7.211e+21
2017-04-29	01:46:00	-72.02	-33.22	24.5	5.41e+16	5.09	4.98e+23	-4.40e+22	-4.54e+23	8.74e+22	-2.43e+23	1.079e+22
2017-04-29	02:36:24	-71.73	-33.12	32.5	7.30e+14	3.84	7.48e+21	-1.76e+21	-5.71e+21	-7.30e+20	2.43e+21	1.489e+21
2017-04-29	04:50:34	-72.07	-33.24	22.5	7.66e+14	3.86	4.21e+21	-9.67e+19	-4.11e+21	3.07e+21	-5.62e+21	6.726e+20
2017-04-29	08:30:43	-72.05	-33.25	24.5	2.92e+15	4.24	8.79e+21	7.25e+21	-1.60e+22	1.38e+22	-2.17e+22	-1.908e+20
2017-04-29	08:54:02	-72.03	-33.24	22.5	2.54e+15	4.20	6.44e+21	4.24e+21	-1.07e+22	8.88e+21	-2.20e+22	1.113e+20
2017-04-30	17:55:34	-72.02	-33.37	26.5	8.74e+14	3.89	5.89e+21	-2.22e+20	-5.67e+21	-6.18e+20	-5.07e+21	-4.335e+21
2017-04-30	21:49:02	-72.26	-32.97	22.5	1.04e+15	3.95	1.05e+22	-1.74e+21	-8.73e+21	4.23e+20	-4.01e+21	-3.070e+20
2017-05-01	23:38:45	-72.21	-33.01	18.5	1.79e+15	4.10	1.49e+22	-1.38e+21	-1.35e+22	1.76e+21	-1.07e+22	-1.596e+20
2017-05-03	16:50:22	-72.26	-33.08	21.5	5.62e+15	4.43	5.74e+22	-1.11e+22	-4.63e+22	2.43e+21	-2.16e+22	1.035e+21
2017-05-04	14:31:43	-72.15	-33.09	22.5	5.62e+14	3.77	4.83e+21	-2.63e+20	-4.57e+21	6.57e+20	-2.99e+21	3.640e+20
2017-05-05	01:34:46	-72.24	-32.90	18.5	1.04e+15	3.95	6.92e+21	5.61e+20	-7.48e+21	8.32e+20	-7.45e+21	9:744e+20
2017-05-05	04:42:01	-71.99	-32.82	22.5	4.92e+14	3.73	2.14e+21	8.61e+19	-2.23e+21	9.84e+20	-4.22e+21	8.527e+20
2017-05-05	10:48:21	-72.18	-32.94	16.5	6.36e+14	3.80	5.53e+21	-1.53e+20	-5.37e+21	1.07e+21	-3.11e+21	-1.131e+20
2017-05-09	09:22:31	-72.27	-33.75	21.5	7.49e+14	3.85	5.79e+21	1.88e+20	-5.98e+21	-4.60e+19	-4.54e+21	9.364e+20
2017-05-09	11:28:32	-72.25	-33.05	19.5	4.44e+14	3.70	4.06e+21	-9.09e+20	-3.15e+21	1.48e+19	-2.55e+21	4.498e+20
2017-05-13	16:54:46	-72.06	-32.94	26.5	6.48e+16	5.14	5.42e+23	-3.86e+22	-5.04e+23	-5.74e+22	-3.78e+23	-6.968e+21
2017-05-16	02:16:29	-72.21	-32.96	16.5	1.99e+15	4.13	-2.93e+21	1.90e+21	1.03e+21	3.93e+21	-1.01e+22	-1.707e+22
2017-05-16	04:36:15	-71.65	-32.00	27.5	4.20e+15	4.35	1.60e+21	9.87e+20	-2.59e+21	2.57e+20	-4.18e+22	3.070e+21
2017-05-18	00:44:56	-72.32	-33.03	17.5	2.20e+15	4.16	2.37e+22	-3.86e+21	-1.98e+22	7.27e+20	-2.60e+21	1.786e+21
2017-05-23	01:05:12	-72.16	-32.94	19.5	1.61e+15	4.07	6.78e+21	-7.61e+20	-6.02e+21	9.26e+21	1.18e+22	1.183e+21
2017-05-29	20:39:36	-71.86	-32.16	26.5	5.78e+14	3.77	-2.65e+21	2.71e+21	-6.71e+19	-1.05e+21	-5.11e+21	1.094e+21
2017-05-30	06:45:58	-72.19	-32.98	18.5	8.59e+14	3.89	7.53e+21	-1.20e+21	-6.34e+21	1.74e+21	-4.68e+21	7.912e+20